HHS Public Access

Author manuscript

Clin Cancer Res. Author manuscript; available in PMC 2019 May 01.

Published in final edited form as:

Clin Cancer Res. 2018 May 01; 24(9): 2159–2170. doi:10.1158/1078-0432.CCR-17-2256.

Concurrent Inhibition of Neurosphere and Monolayer Cells of Pediatric Glioblastoma by Aurora A Inhibitor MLN8237 Predicted Survival Extension in PDOX models

Mari Kogiso[1,2], **Lin Qi**[1,2], **Frank K. Braun**[1,2], **Sarah G. Injac**[1,2], **Linna Zhang**[2], **Yuchen Du**[1,2], **Huiyuan Zhang**[1,2], **Frank Y. Lin**[2], **Sibo Zhao**[1,2], **Holly Lindsay**[1,2], **Jack Su**[2], **Patricia Baxter**[2], **Adesina Adekunle**[3], **Debra Liao**[4], **Mark G. Qian**[4], **Stacey Berg**[2], **Jodi A. Muscal**[2], and **Xiao-Nan Li**[1,2]

[1]Laboratory of Molecular Neuro-Oncology, Texas Children's Hospital, Baylor College of Medicine, Houston, TX, USA

[2]Texas Children's Cancer Center

[3]Department of Pathology, Texas Children's Hospital, Baylor College of Medicine, Houston, TX, USA

[4]Takeda Pharmaceuticals International Co., Cambridge, MA, USA

Abstract

Purpose—Pediatric glioblastoma (pGBM) is highly aggressive tumor in need of novel therapies. Our objective was to demonstrate the therapeutic efficacy of MLN8237 (Alisertib), an orally available selective inhibitor of Aurora A kinase (AURKA), and to evaluate which *in vitro* model system (monolayer or neurosphere) can predict therapeutic efficacy *in vivo*.

Experimental Design—AURKA mRNA expressions were screened with qRT-PCR. *In vitro* anti-tumor effects were examined in 3 matching pairs of monolayer and neurosphere lines established from patient derived orthotopic xenograft (PDOX) models of the untreated (IC-4687GBM), recurrent (IC-372GBM) and terminal (IC-R0315GBM) tumors; and *in vivo* therapeutic efficacy through log rank analysis of survival times in 2 models (IC-4687GBM and IC-R0315GBM) following MLN8237 treatment (30 mg/kg/day, *p.o.*,12 days). Drug concentrations *in vivo*, mechanism of action and resistance were also investigated.

Results—AURKA mRNA over-expression was detected in 14 pGBM tumors, 10 PDOX models and 6 cultured pGBM lines as compared with 11 low grade gliomas and normal brains. MLN8237 penetrated into pGBM xenografts in mouse brains. Significant extension of survival times were achieved in IC-4687GBM of which both neurosphere and monolayer were inhibited *in vitro*, but not in IC-R0315GBM of which only neurosphere cells responded (similar to IC-3752GBM cells). Apoptosis mediated MLN8237 induced cell death, and the presence of AURKA-negative and $CD133^{+}$ cells appears to have contributed to *in vivo* therapy resistance.

Corresponding author: Xiao-Nan Li, M.D., Ph.D., Texas Children's Cancer Center, 1102 Bates, Suite 1030.11, Houston, TX 77030; Phone: 832-824-4580; Fax 832-825-4038; xiaonan@bcm.edu.

Conflict of Interest: Debra Liao and Mark G. Qian are employees of Takeda Pharmaceuticals. Other authors declare no potential conflicts of interest.

Conclusions—MLN8237 successfully targeted AURKA in a subset of pGBMs. Our data suggest that combination therapy should aim at AURKA-negative and/or $CD133^+$ pGBM cells to prevent tumor recurrence.

Keywords

Aurora A kinase; MLN8237; glioblastoma; CD133; orthotopic xenograft

Introduction

Glioblastoma (GBM) is one of the most malignant brain tumors that occurs in adults and children. Unlike adult GBM in which the standard treatment is radiation therapy and adjuvant Temozolomide (1), a standard of care does not exist for the treatment of pediatric GBM (pGBM) (2). The five–year survival rate in patients with pGBM remains at 20% (3). Novel therapy for this disease is critically needed.

Recent studies suggest Aurora A serine/threonine kinases as potential oncologic targets (4, 5). Of the three related Aurora kinases (Aurora A, B, and C) (6), Aurora A kinase (AURKA) regulates centrosome maturation, mitotic entry, centrosome separation, spindle formation, and cytokinesis (4). Amplification and/or overexpression of AURKA has been reported in multiple human tumors (7–14). In central nervous system tumors, AURKA overexpression correlates with disease progression and shorter survival times (15–17). Among the newly developed AURKA inhibitors, MLN8237 (Alisertib) is an orally available reversible selective inhibitor with strong antitumor activity both *in vitro* and *in vivo* (12, 17–22). Additionally, MLN8237 passes through the blood-brain barrier (BBB), and thus is an attractive agent to treat CNS malignancies (23). One of the key mechanisms of MLN8237-induced cell death is upregulation of p53 (11, 19). Since p53 mutation is far less frequent in pGBM than in adult GBM (24, 25) and MLN8237 exhibited an acceptable safety profile in adult and pediatric phase I/II trials (26–30), the applicability of MLN8237 can potentially be greater and expedited in pGBM tumors.

As the incidence of pGBM is less than adult GBM and the number of available new candidate treatment agents is increasing, it is important to establish strong preclinical rational to prioritize new agents for a clinical trial, and more importantly, to improve the chances of clinical success. For initial drug screening, it is desirable to develop an *in vitro* drug testing system that can predict *in vivo* efficacy in animal models. In addition to traditional monolayer cultures, new 3-dimensional (3D) cultures, such as spheroids and organoids (31), have been developed. While neurospheres better represent 3D tumor architecture, microenvironment, and cellular heterogeneity of patient tumor and favor the growth of cancer stem cells (CSCs), the lack of paired neurosphere and monolayer cultures derived from the same patient makes it difficult to determine which culture type better predicts *in vivo* treatment response or if tumor cells in both cultures need to be targeted. For the subsequent *in vivo* evaluation of therapeutic efficacy, it is ideal to include model systems derived from tumors at different points of disease presentation. For example, therapies that are effective in treatment-naïve animal models frequently fail in the heavily pretreated patients with refractory tumors who are the subjects of most early phase clinical trials. While

conversely, testing new drugs in comparatively resistant tumor models jeopardizes discounting new therapies which may prove effective in the context of upfront therapy.

We have optimized a surgical procedure that allows for the safe and rapid implantation of pediatric brain tumor cells into the matching locations in the brains of severe combined immunodeficiency (SCID) mice (32–36). Our detailed characterization of these patient-derived orthotropic xenograft (PDOX) mouse models has confirmed their faithful replication of histopathological features, invasive phenotypes, and major genetic abnormalities of the original patient tumors (32–36). From PDOX tumors of pGBM, we also established 3 matching pairs of cultured monolayer and neurospheres to facilitate the *in vitro* and *in vivo* evaluation of new therapies, such as MLN8237 in pGBMs.

In this report, we evaluated AURKA expression in pGBMs compared to pediatric low grade gliomas, examined the *in vitro* antitumor effects of MLN8237 by treating paired monolayer and neurosphere cultures established from three pGBM models derived from untreated, recurrent, and terminal/lethal tumors, performed detailed analyses of *in vivo* therapeutic efficacy, and determined mechanisms of action of MLN8237 in two pGBM models. Our objectives were to examine if AURKA is a therapeutic target in pGBM, if MLN8237 can effectively target this deadly disease, and if effective targeting of both monolayer and neurosphere cells predicts prolonged animal survival time.

Materials and Methods

Pediatric glioma tumors

Fresh tumor tissue was collected from 11 patients with low grade gliomas (LGG) (WHO grade I/II) and 14 patients with pGBMs (WHO grade IV). Signed informed consent was obtained from the patient or legal guardian prior to sample acquisition in accordance with Institutional Review Board (IRB) policy. All studies were conducted in accordance with the ethical guideline of Declaration of Helsinki. Normal control human cerebellar RNAs from 5 adult as well as total RNAs from 2 fetal brains was procured from a commercial source (Clontech Laboratories, Inc., Mountain View, CA and Biochain, Hayward, CA) (37).

Patient-derived orthotopic xenograft (PDOX) mouse models

Orthotopic free-hand surgical transplantation of tumor cells into mouse cerebrum was performed as we have described previously (36) following an Institutional Animal Care and Use Committee-approved protocol. PDOX (or orthotopic PDX, oPDX) models of intra-cerebral (IC)-4687GBM, IC-3752GBM (38) and IC-R0315GBM were established by direct injection of surgical or autopsy specimens into mouse cerebra; maintenance of reproducible tumorigenicity was confirmed for 5 *in vivo* passages. These xenograft tumors replicated major histopathological features of the original patient tumors (38), and all three models are highly invasive in mouse brains. Patient tumor 4687GBM was obtained at the time of initial tumor resection (therapy-naïve), while patients 3752GBM and R0315GBM were heavily treated prior to sample acquisition (Table 1). The non-obese diabetic (NOD)/SCID mice were maintained in a pathogen-free animal facility at Texas Children’s Hospital. Mice of both sexes, aged 6–8 weeks, were anesthetized with sodium pentobarbital (50 mg/kg).

Tumor cells (1×10^5), isolated from donor xenografts, were suspended in 2 μL of culture medium and injected into the cerebral hemisphere (1 mm to the right of the midline, 1.5 mm anterior to the lambdoid suture, and 3 mm deep) with a 10-μL 26-gauge Hamilton Gastight 1701 syringe needle.

Growth of matched pairs of monolayer and 3D neurosphere cultures from PDOX pGBM cells

Three pairs of cultured pGBM cells were initiated from tumors harvested from PDOX models and established as both monolayer and neurosphere cultures (32, 39). Monolayer cells were cultured in DMEM media supplemented with 10% fetal bovine serum (Atlanta Biologicals, Inc., Flowery Branch, GA), 200 units/mL penicillin/streptomycin. Neurosphere cells, in which putative cancer stem cell populations are enriched, were cultured in serum-free cell growth medium consisting of Neurobasal media, N2 and B27 supplements (Life Technologies, Grand Island, NY), recombinant human βFGF and EGF (50 ng/mL each; R&D Systems Inc., Minneapolis, MN), 200 units/mL penicillin/streptomycin (32, 39).

Quantitative Real-time PCR

Total RNA was extracted with TRIzol reagent (Invitrogen, Carlsbad, CA) from snap frozen patient and xenograft tumor tissue and cultured cell lines. cDNA synthesis from 1μg of total RNA was performed using High Capacity RNA-to-cDNA Kit (Applied Biosystems, Foster City, CA) following manufacturer's protocol. Gene-specific quantitative RT-PCR analysis of AURKA was performed with SYBR select master mix (Applied Biosystems) on a StepOnePlus Real-Time PCR system and MicroAmp Fast optical 96-well reaction plate (Applied Biosystems) using synthesized 5 ng cDNA. The following primers were used: AURKA=Forward 5′-CTGCATTTCAGGACCTGTTAAGG-3', Reverse 5'-AACGCGCTG GGAAGAATTT-3' (40) and GAPDH=Forward 5'-AAGGTGAA GGTCGGAGTCAA-3', Reverse 5'-AATGAAGGGGTCATTGATGG-3'. Relative mRNA expression levels against normal pediatric/adult cerebral tissues were determined by the 2-ΔΔCt method. All quantitative RT-PCR assays were performed in triplicate.

In vitro treatment with MLN8237

MLN8237, provided by Millennium Pharmaceuticals, Inc. (Cambridge, MA), was dissolved in dimethyl sulfoxide for a stock solution of 10 mM for *in vitro* experiments. To determine the time- and dose-dependent effects of MLN8237, paired pGBM monolayer and neurosphere cultures were seeded into 96-well plates and exposed to 7 doses of MLN8237 (ranging from 1-4,000 nM) or vehicle control over a 2 week period. Cell viability was measured at day 1, 4, 7, 10, and 13 using the Cell Counting Kit-8 (CCK8) (Dojindo Molecular Technologies, Rockville, MD) (32, 35).

In vivo treatment of PDOX tumors with MLN8237

For *in vivo* experiments, MLN8237 was dissolved in 10% (2-Hydroxypropyl)-β-cyclodextrin (Sigma-Aldrich)/1% sodium bicarbonate to achieve a final concentration of 5 mg/mL. Two weeks after intra-cerebral tumor cell implantation, mice were orally administered MLN8237 (30 mg/kg/day) (19, 23, 41, 42) once daily for 12 days. To

determine any survival benefits from MLN8237 treatment, the mice were monitored daily until they developed signs of neurological deficit or became moribund, at which time they were euthanized and their brains removed for analysis. To test the biologic effects of MLN8237 at the end of treatment, mice were treated with MLN8237 (30 mg/kg/day), a dose frequently used before in animal experiments (19, 23, 41, 42) for 12 days once initial neurologic symptoms caused by GBM growth were observed; these mice were euthanized 1, 24 and 72 hours after the last MLN8237 dose, and their brains were removed for analysis. Plasma was collected from all euthanized mice.

Flow cytometry (FCM)

Flow cytometry was performed as we described previously (32, 35, 36, 38). To examine the changes in cell cycle distribution, tumor cells were washed and incubated at 37°C for 45 minutes with 10 μg/mL Hoechst 33342 (Sigma-Aldrich) and Verapamil (ATP pump inhibitor, 50μM) in FCM buffer (Dulbecco's phosphate-buffered saline, 0.5% BSA and 2 mM EDTA) for DNA staining following incubation with 0.5 μg/mL PyroninY (Sigma-Aldrich) for another 45 minutes to stain RNA. To exclude mouse cells from analysis, xenograft cells were stained with a cocktail of APC-conjugated antibodies specific to mouse cell surface antigen (CD90.1, CD133, CD140a and CD24) together with matching APC-conjugated isotype control antibodies (Mouse IgG1 κ, Rat IgG2a κ and Rat IgG2b κ) (BioLegend, Inc., San Diego, CA) to set the gate. To analyze the putative CSCs, tumor cells were washed and labeled with APC-conjugated anti-human CD133 (Miltenyi Biotech Inc, San Diego, CA) and FITC-conjugated anti-human CD15 (Miltenyi Biotech Inc) for 15 minutes on ice in 100 μL of FCM buffer containing FcR Blocking Reagent (32, 35, 36, 38). Anti-mouse IgG2b-APC and anti-mouse IgM-FITC antibodies (Miltenyi Biotech Inc) were also included as isotype controls. After washing, cells were resuspended in FCM buffer containing 2 μg/mL PI to gate out dead cells and analyzed with a LSR II flow cytometer and Kaluza Analysis Software Version 1.3 (Beckman Coulter, Inc., Brea, CA).

MLN8237 concentration in plasma, tumor, and normal brain

MLN8237 concentrations were determined using an Applied Biosystems API5000 mass spectrometer equipped with a Shimadzu Nexera UFLC System and a LEAP autosampler following an optimized method at Takeda Pharmaceuticals. A reversed-phase gradient method with flow rate of 0.4 mL/min on a Phenomenex Synergi Polar-RP column was used for analyte separation. The mobile phases used were water and acetonitrile (supplemented with formic acid 0.1% volume-to-volume). MLN8237 was ionized under a positive ion spray mode and detected through the multiple-reaction monitoring of a mass transition pair at a mass-to-charge ratio of 519.1/328.1. Calibration curves of MLN8237 were established using standards, and the peak area ratios of the analyte against an isotopically-labeled internal standard were used to quantify samples. Using a plasma volume of 50 μL, linearity was achieved in the MLN8237 concentration range of 1.93-3860 nM. In addition, dilution linearity was also assessed to ensure that study samples above the upper limit of the standard curve could be diluted with blank matrix without affecting the final calculated concentration. This was performed by preparing dilution QC's at 19300 nM and diluting down to the curve range by 50 fold with blank mouse plasma. The triplicate dilution QC's have met the acceptance criteria of within 15% with respect to accuracy and precision. This approach

validated the dilution cap of accurately quantifying samples that are AQL (Above Quantitation Limit) up to 19300 nM. All data were acquired and processed using Analyst 1.6.2 software (Applied Biosystems).

Western hybridization

Proteins were extracted in M-PER Mammalian Protein Extraction Reagent (Life Technologies) including Protease Inhibitor Cocktail, separated with SDS-PAGE in a 4-12% Bis-Tris-Gel, transferred to nitrocellulose membrane, and incubated with the primary antibodies: Anti-Aurora A (1:1000, Cell Signaling Technology, catalog# 4718), anti-PARP (recognizes both the full and the cleaved fragment, 1:500, Calbiochem, catalog# AM30), anti-caspase-3 (recognizes both the full and the cleaved fragments, 1:1000, Cell Signaling Technology, catalog# 9662) and anti-β-actin (1:5000, Sigma-Aldrich, catalog# A2228). Following incubation with IRDye-conjugated secondary antibody (1:10,000, LI-COR Biosciences), proteins were detected and quantitated using an Odyssey Infrared Imaging System (LI-COR Biosciences) application Software version 3.0.

Immunohistochemical Staining (IHC)

IHC staining was performed using a Vectastain Elite ABC kit Rabbit IgG (Vector Laboratories, Burlingame, CA) or Mouse on Mouse (M.O.M.) Elite Peroxidase Kit (Vector Laboratories) on 5 μm paraffin sections of whole mouse brains as described previously (32, 35, 36, 43). After antigen retrieval with Target Retrieval Solution (Dako North America, Inc., Carpinteria, CA) in a pressure cooker, sections were blocked with horse normal serum or M.O.M. Mouse IgG Blocking Reagent. Primary antibodies utilized were full PARP (1:100) (Sigma-Aldrich), cleaved PARP (1:100), full caspase-3 (1:50), cleaved caspase-3 (1:100), AURKA (1:50) (Cell Signaling Technology, Inc.), and Ki67 (1:50) (Abcam, Cambridge, MA). After slides were incubated with primary antibodies, appropriate biotinylated secondary antibodies were applied, and the final signal was developed using 3, 3′-diaminobenzidine substrate kit for peroxidase. Negative control was performed by replacing primary antibodies with Dulbecco's phosphate-buffered saline. IHC staining was assessed by combining intensity, scored as negative (–), low (+), medium (++), or strongly positive (+++), with extent of immunopositivity (percentage of positive cells). For AURKA, the immunohistochemistry H-score was calculated as 3 x percentage of strong (+++) positive cells + 2 x medium (++) positive cells + 1 x low (+) positive cells (44).

Statistical Analysis

Values were presented as mean ± standard deviation (SD). The effect on cell proliferation was analyzed with two-way analysis of variance (ANOVA), and *in vitro* cell cycle analyzed with one-way ANOVA followed by a multiple comparison procedure (Holm-Sidak method). Animal survival times were compared through log-rank analysis. *In vivo* cell cycle and CSC populations were analyzed with pair-wise t-test. All statistical analysis was performed by using SigmaStat 3.5 (Systat Software, Inc., San Jose, CA). $P < 0.05$ was considered statistically significant.

Results

AURKA was overexpressed in pGBM tumor, PDOX models, and cultured cells

To evaluate AURKA mRNA expression in pGBMs, q-RT PCR was performed on patient samples from 11 pediatric LGGs, 14 pGBMs and 7 normal cerebral tissues. Consistent with previous observations (17), AURKA mRNA was significantly overexpressed in pGBM with a mean tumor/normal ratio of 12.50±7.98 compared to LGG (1.67±0.68) and normal cerebral tissue (1.60±1.71) ($P<0.05$) (Fig. 1A). Subsequent evaluation of 10 PDOX pGBM mouse models and 3 pairs of patient-matched monolayer and neurosphere cultures derived from PDOX models of pGBM confirmed the maintenance of AURKA mRNA overexpression in xenograft tumors (up to 5 *in vivo* passages) (Fig. 1B) and in the cultured pGBM cells (Fig. 1C).

MLN8237 inhibited cell proliferation *in vitro* in neurospheres and monolayer cells

To evaluate AURKA as a potential therapeutic target in pGBM, we examined *in vitro* effects of MLN8237 using cell cultures derived from 3 PDOX models (Table 1) representing different clinical timepoints of disease progression, i.e., previously untreated (IC-4687GBM), recurrent following treatment (IC-3752GBM), and a progressive, terminal stage obtained at autopsy (IC-R0315GBM). Recognizing the role of CSCs in the progression and recurrence of GBM (45), stem-cell enriched neurosphere cell lines were treated together with the matching monolayer cells to MLN8237 (1-4,000 nM).

In CSC-enriched neurospheres, MLN8237 showed significant inhibition of growth at nanomolar concentrations in all 3 lines in a time- and dose-dependent manner (Fig. 2A and Fig. S1). Neurospheres from previously untreated patient tumor (IC-4687GBM) were the most sensitive to treatment with MLN8237, demonstrating significant suppression of cell proliferation after treatment with 15.6 nM of MLN8237 from day 4 (28.2 ± 6.7%) through day 13 (>90%). In the recurrent model IC-3752GBM, the cells were more resistant to treatment as 62.5 nM of MLN8237 led to 45.9 ± 6.2% growth suppression on day 7 and 75 ± 0.6% inhibition on day 13. In the autopsy/terminal model IC-R0315GBM, treatment with 62.5 nM of MLN8237 resulted in >95% suppression of cell proliferation from day 7 to 13 ($P<0.05$). In monolayer cell lines, only the IC-4687GBM cells (previously untreated) were sensitive to MLN8237, but it required a higher dose (250 nM) and longer exposure (day 7) to achieve >90% inhibition. Monolayer cells derived from the recurrent and terminal GBM models were resistant to MLN8237, and <50% inhibition was achieved even with 4,000 nM for 13 days. Worthy of note is that monolayer cells from IC-4687GBM proliferated much faster than the other 2 models, which may partially explain their early responses to MLN8237. Overall, these data identified the treatment naïve IC-4687GBM as the most responsive tumor model and revealed differential responses between neurosphere and monolayer cells in the recurrent and terminal pGBM models.

MLN8237 induced apoptosis in pGBM cells *in vitro*

To examine the drug's mechanism of action, first we examined apoptosis *in vitro* through FCM. To examine time-course responses, pGBM cells were treated with MLN8237 at 62.5 nM, a dose active in neurospheres from all 3 models, for 1–7 days. In neurospheres,

significantly elevated apoptosis (% of cells in Sub-G_1) (P<0.05) was observed on day 2 (20%) in IC-4687GBM, day 4 (40%) in IC-3752GBM, and day 1 (18%) in IC-R0315GBM. The levels of apoptosis increased over time and peaked on day 7 reaching 65-75% (Fig. 2C). In monolayer cells, only moderate apoptosis was noted in IC-3752GBM (18% on day 1, 25% on day 7). In agreement with these data, Western hybridization demonstrated similar results with dose-dependent cleavage of PARP detected in all neurosphere cultures but minimal effects observed in the monolayer cells, including a minor effect on caspase 3 (Fig. 2D). To examine dose responses, cells were treated with MLN8237 (4, 62.5 and 1,000 nM) (Fig. 2A) and analyzed by FCM on day 7 of treatment, a point at which growth inhibition was observed in the CCK8 assays. In neurospheres, a significant increase in the sub-G_1 population was observed on day 7 with 4 nM of MLN8237 in IC-4687GBM (15%), and treatment with 62.5 nM and higher resulted in more significant increases (60-90%) in apoptosis in all 3 models. However, in monolayer cells, higher drug doses (e.g. 1,000 nM in IC-4687GBM) were required to induce even lower levels of apoptosis (e.g. 60% in IC-4687GBM) (Fig. 2C). Overall, MLN8237 induced significant apoptosis in pGBM cells, particularly in the neurospheres.

Next we analyzed changes in cell cycle distribution in viable tumor cells *in vitro* by excluding the sub-G_1 population (Fig. 2B). In neurospheres, a time course treatment with 62.5 nM of MLN8237 revealed early (day 1-2) reduction of G_0/G_1 phase cells accompanied by accumulation of G_2/M phase cells in all 3 models (Fig. S2A, *right panel*). Prolonged treatment to day 7 resulted in release of G_2/M blockage and an increase in G_0/G_1 phase cells. Analysis of dose responses on day 7 failed to detect dose-dependent G_2/M block (Fig. S2A, *left panel*). In monolayer cells, time-course analysis detected G_0/G_1 reduction and G_2/M block in IC-3752GBM (recurrent) and IC-R0315GBM (autopsy) cells, but not in IC-4687GBM (treatment naive) (Fig. S2A, *right panel*). Also IC-3752GBM was the only model that displayed a dose-dependent G_0/G_1 decrease (from 80% to 38%) and G_2/M blockage (from 10% to 60%) at 1,000 nM (Fig. S2A, *left panel*). These data indicated that MLN8237 was able to induce short-term (1-2 days) G_2/M blockage in pGBM neurospheres but failed to trigger major responses in monolayer cells from the 3 models.

MLN8237 effectively crosses the blood-brain barrier (BBB) in PDOX models of pGBM

One major hurdle in the treatment of CNS tumors is the necessity for drugs to cross the BBB. Before we launch a large scale *in vivo* efficacy examination, we examined the CNS penetration capability of MLN8237 in a responsive pGBM by treating IC-4687GBM with MLN8237 for 12 days (30 mg/kg/day) (Fig. 3A). Drug levels in xenograft tumors were compared to levels in the neighboring “normal” mouse brains and in the serum (Fig. 3B). In plasma, MLN8237 was detected at a concentration of 6,636 ± 1,687 nM (n=6) 1 hour following the completion of treatment and decreased to 1,126 ± 546 nM at 24 hours (n=4) and to undetectable levels (< 1 nM) at 72 hours (Fig. 3B). Compared with levels of MLN8237 in the normal mouse brain tissues (397 ± 100 nM) (n=2) at 1 hour post-treatment and (45 ± 4 nM) (n=2) at 24 hour post-treatment, MLN8237 accumulated in tumor tissue to 615 nM (n=1) at 1 hour and remained elevated at 90 nM (n=1) at 24 hours post-treatment (Fig. 3B). Worthy of note is that this tumor is highly invasive. Therefore, the normal tissues harvested from the tumor bearing mice may contain small amount of invasive tumor cells.

The significantly elevated drug concentration in the tumor mass indicated that MLN8237 was able to penetrate the BBB and accumulate in IC-4687GBM. Compared with serum concentrations achieved in adults in a phase I trial (approximately 5,000 nM ± 1,800 nM, 7 days at 100 mg/kg, twice daily), the serum concentration in our animals are slightly higher (27).

MLN8237 prolonged animal survival times through induction of apoptosis

We next examined the activity of MLN8237 *in vivo* and assessed if *in vitro* activity predicted the *in vivo* therapeutic efficacy. Specifically, we examined if effective targeting of CSC-enriched neurospheres (38, 46–49) was sufficient to predict significant extension of animal survival times or if simultaneous targeting of both neurospheres and monolayers was required. Mice bearing IC-4687GBM (previously untreated pGBM with monolayer and neurosphere MLN8237 sensitivity) and IC-R0315GBM (terminal pGBM with only neurosphere MLN8237 sensitivity) were orally treated with MLN8237 (30 mg/kg/day for 12 days) 2 weeks after tumor implantation. Animal survival times (median) in IC-4687GBM were significantly prolonged from 53 days in the vehicle group to 78 days in the treatment group (P=0.022) (Fig. 3C). However, in the autopsy model IC-R0315GBM, the median survival time was 41 days in vehicle group and 42 days in the MLN8237-treated group (*P*=0.859). While these data suggested that simultaneous suppression of both neurospheres and monolayer cells correlates with improved therapeutic efficacy while *in vitro* suppression of neurospheres alone was insufficient to extend animal survival times, additional studies are needed in more tumor models to validate the power of paired monolayer and neurosphere cultures in predicting *in vivo* success of drug treatment.

Since our *in vitro* data showed that MLN8237 induced apoptosis, we validated the role of apoptosis *in vivo* in mice 1 hours post-drug treatment (acute response) and in the recurrent tumors in the survival group (long-term/delayed effects). In the responsive model IC-4687GBM, MLN8237 (30 mg/kg/day for 12 days by gavage) resulted in significant increases in apoptosis (1 hours after completion of treatment) as evidenced by increased cleaved PARP (from + in ≤25% cells to +++ in nearly 75% of cells), cleaved caspase-3 (from ++ in ≤25% cells to +++ in 50-75% cells) (Fig. 3D and Table 2), and accumulation of cells in the $SubG_1$ phase from pretreatment (3.6± 0.4%) to 1 hours after completion of treatment (10.4 ± 1.9%) (Fig. 3E). As anticipated, in the cells from recurrent tumor (harvested in the survival group), cleaved PARP and cleaved caspase-3 decreased to low levels similar to baseline (+ in ≤25% cells and $SubG_1$ to 3.1 ± 1.5%). Parallel to the increased apoptosis, changes of histological features, such as decreased cell density (Fig. 3F) and increase of cell size (Fig. 3D, H&E staining), were also noted. In the autopsy model IC-R0315GBM, elevated cleavage of PARP and caspase-3 were only found in <25% cells. In all the tumor cells in both models, a high level (+++) expression of full PARP and caspase-3 was maintained, suggesting that surviving cells had functional apoptotic machinery. Cell proliferation (Ki-67) was not significantly altered at any timepoints in either model.

Tumor cells lacking AURKA expression survived MLN8237 treatment *in vivo*

Despite significant prolongation of survival times following MLN8237 treatment in IC-4687GBM mice, all animals in our study ultimately succumbed to their tumors. To

understand the mechanisms of therapy resistance, we examined changes of AURKA (molecular target of MLN8237) through IHC and evaluated as H-score, calculated as 3 x percentage of strong (+++) positive cells + 2 x medium (++) positive cells + 1 x low (+) positive cells (44) (Fig. S3A). Compared with vehicle-treated IC-4687GBM tumors with H-score 19.8 ± 4.8 for AURKA, it decreased to 8.8 ± 4.4 (P<0.001) with many areas lacking AURKA expression in recurrent tumors. There was no change in the H-score at the end of treatment tumor (22.4 ± 9.4) compared to vehicle-treated IC-4687GBM. In the resistant model IC-R0315GBM, cells with strong (+++) or medium (++) positivity decreased while low (+) positive cells slightly increased in the recurrent tumor (Fig. S3B). These data suggest that pGBM tumor cells with low or no AURKA expression escaped MLN8237-induced cell killing and contributed to progression and recurrence of xenograft tumors in these two pGBM models, although data from additional models are needed to draw a definitive conclusion.

In vivo tumor progression was associated with persistence of CD133$^+$ cells

Next we examined the role of CSCs using FCM analysis of dual-stained CD133$^+$ and CD15$^+$ cells, the two most commonly utilized cell surface markers for brain tumor stem cells in both neurospheres and xenografts. *In vitro*, CD133$^+$CD15$^-$ cells represented the major population of neurosphere cells derived from both IC-4687GBM (36.1%) and IC-R0315GBM (57.2%) (Fig. 4A). Treatment with MLN8237 (4-62.5 nM) for 7 days resulted in a minor shift (≤7%) of the mono (CD133$^+$CD15$^-$ and CD133$^-$CD15$^+$) and dual (CD133$^+$CD15$^+$) sub-populations, suggesting that all subpopulations were similarly, if not equally, sensitive to MLN8237 treatment. *In vivo* in the MLN8237-responsive model (IC-4687GBM), we detected an increase of mono-CD133$^+$ (CD133$^+$CD15$^-$) cells from 9.5 ± 5.9% in vehicle-treated tumors to 28.2 ± 22.2% (P>0.05) in tumors harvested 1 hours after MLN8237 treatment (30 mg/kg x 12 days), and we observed a further increase to 52.3 ± 12.8% (P<0.05) in the recurrent tumors (Fig. 4B). These changes were accompanied by a steady decrease of CD15-mono positive (CD133$^-$CD15$^+$) cells (P=0.055) whereas changes of dual-positive (CD133$^+$CD15$^+$) cells were not significant (Fig. 4B). Progressive tumors from the MLN8237-resistant model (IC-R0315GBM) showed similar enrichment of CD133$^+$ cells (69.8 ± 8.6% in vehicle and 80.8 ± 0.0% in MLN8237-treated group) (P<0.05). However, the majority of the xenograft CD133$^+$ cells in IC-R0315GBM co-expressed CD15 (59.4 ± 7.6% in vehicle and 76.2 ± 0.0% in MLN8237-treated group) (Fig. 4B, *lower panel*), which was significantly different from the neurospheres that were predominantly CD133-mono-positive (CD133$^+$CD15$^-$) (Fig 4A, *lower panel*). In summary, these data suggest that the putative CSC population *in vitro* in cultured neurosphere cells did not have identical responsiveness toward MLN8237 as the CSCs in xenograft tumors, and CD133$^+$ cell were the cause of therapy resistance because nearly all the CD15$^+$ cells were dual positive with CD133.

Discussion

In this report, we identified AURKA as a potential therapeutic target in a subset of pGBM by validating its overexpression in patient tumors, PDOX models, and matching pairs of cultured neurosphere and monolayer cultures of pGBM. We demonstrated strong antitumor

activity of the AURKA inhibitor MLN8237 *in vitro* and *in vivo* and identified variable responses in pGBM cells derived from different stage of clinical progression (treatment naïve, recurrence, and terminal/autopsy) and between matching pairs of neurospheres and monolayer cultures. While our data suggested that successful inhibition in both neurosphere and monolayer cells correlates with extension of animal survival times, additional studies involving more tumor models are needed to further test the "adherent versus spheroid" hypothesis and to correlate with the frequent molecular changes. Mechanistically, we confirmed apoptosis as the primary cause of MLN8237-induced cell death and suggested the lack of AURKA expression and the expression of CSC marker CD133 as causes of therapy resistance. These findings also support a secondary transplantation of the treated (resistant) tumor cells followed by another round of AURKA inhibitor treatment to confirm the sustained resistance of the AURKA-negative and/or $CD133^+$ cells toward AURKA inhibition in pGBMs.

Overexpression of AURKA and preclinical antitumor activity of AURKA inhibitors have been reported extensively in various human cancers. AURKA inhibitor MLN8237 (alisertib) is orally available and has exhibited strong antitumor activity in a wide range of human cancers and has a well-established clinical safety profile (26–30, 50, 51). The advantage of preclinical testing of therapeutic efficacy in PDOX models of pGBM, a disease that desperately needs new therapies, is that *in vivo* findings can potentially be rapidly translated into clinical trials. In an effort to facilitate the initiation of clinical trials, we address two important issues. First we examined the treatment effects in samples from different stages of clinical progression and how *in vitro* models predict *in vivo* efficacy. Using our unique panel of PDOX models of pGBM, we examined the impact of clinical timepoint of the original patient tumor on the overall response to treatment with MLN8237. Although these models were not derived from the same patients (which is highly desired but very difficult to accomplish), testing new therapies in models representing untreated, recurrent, and terminal/autopsy pGBMs can provide important clues for future selection of patients. Our findings that previously treated recurrent and autopsy pGBM models responded differently to MLN8237 compared to the treatment naïve tumor model suggests a need for a broader range of tumor models in future preclinical drug testing.

Second, since *in vivo* evaluation of therapeutic efficacy can be both time consuming and costly, *in vitro* prescreening assays that can better predict *in vivo* success are highly desired. Unlike traditional monolayer cells, neurospheres are enriched with CSCs, making them frequently favored over monolayer cells for *in vitro* preclinical drug testing (22, 52). Using AURKA-overexpressing neurosphere and monolayer pGBM lines, we found that MLN8237 was effective in reducing growth in all 3 neurosphere cultures enriched with putative glioma stem ($CD133^+$ and $CD15^+$) cells; these results are similar to preclinical findings in adult GBMs (21, 52). Unexpectedly, monolayer cultures were less responsive to MLN8237 treatment despite expressing similarly high levels of AURKA. Our data demonstrates that tumor cells maintained in these two growth conditions did not always respond identically to the same treatment, and that when MLN8237 effectively suppressed both neurosphere and monolayer cells *in vitro*, the xenograft models demonstrated the most significant *in vivo* drug responses. These data support the inclusion and testing of both monolayer and neurosphere cells in future drug development to validate the predictability of this strategy.

Similar to many previous studies on the molecular mechanisms of action of MLN8237 (11, 19, 22, 53–56), we demonstrated that apoptosis and cell cycle arrest in G_2/M phase mediated the antitumor activity in pGBM both *in vitro* and *in vivo*. Despite the significantly prolonged animal survival time in IC-4687GBM, all the animals in the treatment group died of disease. To further understand the mechanisms of therapy resistance, we analyzed the protein expression of AURKA, the target of MLN8237, in the remnant/recurrent xenograft tumors through IHC. Not surprisingly, the number of AURKA-positive cells was dramatically decreased in the remnant/recurrent tumors, suggesting that 12 days of treatment with MLN8237 successfully eliminates AURKA-positive tumor cells, and implying that the AURKA-negative tumor cells that escaped MLN8237 treatment caused tumor recurrence/progression. This finding supports additional studies to establish the role of AURKA levels in determine drug responsiveness, e.g. by showing that knockdown of AURKA levels *in vitro* results in a shift of drug potency. Since high expression of full PARP and caspase-3 was detected in the remnant/recurrent tumors, these residual tumor cells may have functional apoptotic machinery that can be targeted in the future development of combination therapy with MLN8237 (22, 57–61).

Additionally, our study of the mechanisms of resistance provided new insights on the role of CSCs in MLN8237 resistance. In IC-4687GBM, although CD133 and CD15 (both mono- and dual-positive) cells were killed by MLN8237 in neurospheres *in vitro*, the fraction of CD133-mono positive cells increased in the remnant/recurrent xenografts *in vivo*. In IC-R0315GBM, while CSCs in neurospheres were predominately (>50%) composed of CD133-mono positive ($CD133^+CD15^-$) cells, the xenografts were dual positive ($CD133^+CD15^+$) cells (59.4% before treatment and 76.2% in recurrent tumor). Such cellular differences, likely caused by changes in microenvironment, may have contributed to the differential responses observed in this terminal stage pGBM model. This finding suggests that serum-free cell culture may favor the growth of a subpopulation of stem cells which may not accurately reflect *in vivo* behavior. Our data shows that some pGBM cells expressing CD133 (alone or with CD15) were resistant to MLN8237 *in vivo*, and new strategies capable of effectively targeting CSCs are needed to further enhance the *in vivo* efficacy of MLN8237.

In conclusion, we identified AURKA as a novel therapeutic target for pGBM and demonstrated the strong antitumor activity of MLN8237 *in vitro* in neurospheres and *in vivo* in a treatment naïve PDOX model. Also this study suggested that simultaneous targeting of neurosphere and monolayer cell lines correlates with prolonged animal survival *in vivo*. Our data also support additional *in vivo* studies to confirm the loss of molecular target AURKA and increased expression of CD133 by tumor cells as the mechanisms of MLN8237 resistance in pGBM cells. Our data suggests that combination therapy is required to target AURKA-negative fractions and $CD133^+$ cells following treatment with AURKA inhibition to further improve therapeutic efficacy.

Supplementary Material

Refer to Web version on PubMed Central for supplementary material.

Acknowledgments

This project is funded by NIH/NCI RO1 CA185402 (XN Li), Cancer Prevention and Research Institute of Texas (CPRIT) RP150032 (XN Li), St Baldrick's Foundation (JM Su), and by the Cytometry and Cell Sorting Core at Baylor College of Medicine with funding from the NIH (P30 AI036211, P30 CA125123, and S10 RR024574), Texas Children's Hospital Pediatric Pilot Award (JAM), Kappa Alpha Theta Foundation Research Scholar (JAM), Alex's Lemonade Stand Center of Excellence (SB).

References

1. Stupp R, Hegi ME, Gilbert MR, Chakravarti A. Chemoradiotherapy in malignant glioma: standard of care and future directions. Journal of clinical oncology : official journal of the American Society of Clinical Oncology. 2007 Sep 10; 25(26):4127–36. [PubMed: 17827463]
2. Fangusaro J, Warren KE. Unclear standard of care for pediatric high grade glioma patients. Journal of neuro-oncology. 2013 Jun; 113(2):341–2. [PubMed: 23471572]
3. Dolecek TA, Propp JM, Stroup NE, Kruchko C. CBTRUS statistical report: primary brain and central nervous system tumors diagnosed in the United States in 2005–2009. Neuro-oncology. 2012 Nov; 14(Suppl 5):v1–49. [PubMed: 23095881]
4. Marumoto T, Zhang D, Saya H. Aurora-A - a guardian of poles. Nature reviews Cancer. 2005 Jan; 5(1):42–50. [PubMed: 15630414]
5. D'Assoro AB, Haddad T, Galanis E. Aurora-A Kinase as a Promising Therapeutic Target in Cancer. Frontiers in oncology. 2015; 5:295. [PubMed: 26779440]
6. Carvajal RD, Tse A, Schwartz GK. Aurora kinases: new targets for cancer therapy. Clinical cancer research : an official journal of the American Association for Cancer Research. 2006 Dec 1; 12(23): 6869–75. [PubMed: 17145803]
7. Ye D, Garcia-Manero G, Kantarjian HM, Xiao L, Vadhan-Raj S, Fernandez MH, et al. Analysis of Aurora kinase A expression in CD34(+) blast cells isolated from patients with myelodysplastic syndromes and acute myeloid leukemia. J Hematop. 2009 Mar; 2(1):2–8. [PubMed: 19669217]
8. Humme D, Haider A, Mobs M, Mitsui H, Suarez-Farinas M, Ohmatsu H, et al. Aurora Kinase A Is Upregulated in Cutaneous T-Cell Lymphoma and Represents a Potential Therapeutic Target. The Journal of investigative dermatology. 2015 Sep; 135(9):2292–300. [PubMed: 25848977]
9. Ferchichi I, Sassi Hannachi S, Baccar A, Marrakchi Triki R, Cremet JY, Ben Romdhane K, et al. Assessment of Aurora A kinase expression in breast cancer: a tool for early diagnosis? Disease markers. 2013; 34(2):63–9. [PubMed: 23324574]
10. Siggelkow W, Boehm D, Gebhard S, Battista M, Sicking I, Lebrecht A, et al. Expression of aurora kinase A is associated with metastasis-free survival in node-negative breast cancer patients. BMC cancer. 2012; 12:562. [PubMed: 23186136]
11. Zhou N, Singh K, Mir MC, Parker Y, Lindner D, Dreicer R, et al. The investigational Aurora kinase A inhibitor MLN8237 induces defects in cell viability and cell-cycle progression in malignant bladder cancer cells in vitro and in vivo. Clinical cancer research : an official journal of the American Association for Cancer Research. 2013 Apr 1; 19(7):1717–28. [PubMed: 23403633]
12. Sehdev V, Peng D, Soutto M, Washington MK, Revetta F, Ecsedy J, et al. The aurora kinase A inhibitor MLN8237 enhances cisplatin-induced cell death in esophageal adenocarcinoma cells. Molecular cancer therapeutics. 2012 Mar; 11(3):763–74. [PubMed: 22302096]
13. Belt EJ, Brosens RP, Delis-van Diemen PM, Bril H, Tijssen M, van Essen DF, et al. Cell cycle proteins predict recurrence in stage II and III colon cancer. Annals of surgical oncology. 2012 Jul; 19(Suppl 3):S682–92. [PubMed: 22311118]
14. Gritsko TM, Coppola D, Paciga JE, Yang L, Sun M, Shelley SA, et al. Activation and overexpression of centrosome kinase BTAK/Aurora-A in human ovarian cancer. Clinical cancer research : an official journal of the American Association for Cancer Research. 2003 Apr; 9(4): 1420–6. [PubMed: 12684414]
15. Neben K, Korshunov A, Benner A, Wrobel G, Hahn M, Kokocinski F, et al. Microarray-based screening for molecular markers in medulloblastoma revealed STK15 as independent predictor for survival. Cancer research. 2004 May 1; 64(9):3103–11. [PubMed: 15126347]

16. Barton VN, Foreman NK, Donson AM, Birks DK, Handler MH, Vibhakar R. Aurora kinase A as a rational target for therapy in glioblastoma. J Neurosurg Pediatr. 2010 Jul; 6(1):98–105. [PubMed: 20593995]

17. Lehman NL, O'Donnell JP, Whiteley LJ, Stapp RT, Lehman TD, Roszka KM, et al. Aurora A is differentially expressed in gliomas, is associated with patient survival in glioblastoma and is a potential chemotherapeutic target in gliomas. Cell cycle. 2012 Feb 1; 11(3):489–502. [PubMed: 22274399]

18. Maris JM, Morton CL, Gorlick R, Kolb EA, Lock R, Carol H, et al. Initial testing of the aurora kinase A inhibitor MLN8237 by the Pediatric Preclinical Testing Program (PPTP). Pediatr Blood Cancer. 2010 Jul 15; 55(1):26–34. [PubMed: 20108338]

19. Gorgun G, Calabrese E, Hideshima T, Ecsedy J, Perrone G, Mani M, et al. A novel Aurora-A kinase inhibitor MLN8237 induces cytotoxicity and cell-cycle arrest in multiple myeloma. Blood. 2010 Jun 24; 115(25):5202–13. [PubMed: 20382844]

20. Muscal JA, Scorsone KA, Zhang L, Ecsedy JA, Berg SL. Additive effects of vorinostat and MLN8237 in pediatric leukemia, medulloblastoma, and neuroblastoma cell lines. Investigational new drugs. 2013 Feb; 31(1):39–45. [PubMed: 22669335]

21. Mannino M, Gomez-Roman N, Hochegger H, Chalmers AJ. Differential sensitivity of Glioma stem cells to Aurora kinase A inhibitors: implications for stem cell mitosis and centrosome dynamics. Stem Cell Res. 2014 Jul; 13(1):135–43. [PubMed: 24879067]

22. Hong X, O'Donnell JP, Salazar CR, Van Brocklyn JR, Barnett KD, Pearl DK, et al. The selective Aurora-A kinase inhibitor MLN8237 (alisertib) potently inhibits proliferation of glioblastoma neurosphere tumor stem-like cells and potentiates the effects of temozolomide and ionizing radiation. Cancer chemotherapy and pharmacology. 2014 May; 73(5):983–90. [PubMed: 24627220]

23. Hill RM, Kuijper S, Lindsey JC, Petrie K, Schwalbe EC, Barker K, et al. Combined MYC and P53 defects emerge at medulloblastoma relapse and define rapidly progressive, therapeutically targetable disease. Cancer cell. 2015 Jan 12; 27(1):72–84. [PubMed: 25533335]

24. Paugh BS, Qu C, Jones C, Liu Z, Adamowicz-Brice M, Zhang J, et al. Integrated molecular genetic profiling of pediatric high-grade gliomas reveals key differences with the adult disease. Journal of clinical oncology : official journal of the American Society of Clinical Oncology. 2010 Jun 20; 28(18):3061–8. [PubMed: 20479398]

25. Jones C, Perryman L, Hargrave D. Paediatric and adult malignant glioma: close relatives or distant cousins? Nat Rev Clin Oncol. 2012 Jul; 9(7):400–13. [PubMed: 22641364]

26. Dees EC, Cohen RB, von Mehren M, Stinchcombe TE, Liu H, Venkatakrishnan K, et al. Phase I study of aurora A kinase inhibitor MLN8237 in advanced solid tumors: safety, pharmacokinetics, pharmacodynamics, and bioavailability of two oral formulations. Clinical cancer research : an official journal of the American Association for Cancer Research. 2012 Sep 01; 18(17):4775–84. [PubMed: 22767670]

27. Cervantes A, Elez E, Roda D, Ecsedy J, Macarulla T, Venkatakrishnan K, et al. Phase I pharmacokinetic/pharmacodynamic study of MLN8237, an investigational, oral, selective aurora a kinase inhibitor, in patients with advanced solid tumors. Clinical cancer research : an official journal of the American Association for Cancer Research. 2012 Sep 1; 18(17):4764–74. [PubMed: 22753585]

28. Matulonis UA, Sharma S, Ghamande S, Gordon MS, Del Prete SA, Ray-Coquard I, et al. Phase II study of MLN8237 (alisertib), an investigational Aurora A kinase inhibitor, in patients with platinum-resistant or -refractory epithelial ovarian, fallopian tube, or primary peritoneal carcinoma. Gynecologic oncology. 2012 Oct; 127(1):63–9. [PubMed: 22772063]

29. Mosse YP, Lipsitz E, Fox E, Teachey DT, Maris JM, Weigel B, et al. Pediatric phase I trial and pharmacokinetic study of MLN8237, an investigational oral selective small-molecule inhibitor of Aurora kinase A: a Children's Oncology Group Phase I Consortium study. Clinical cancer research : an official journal of the American Association for Cancer Research. 2012 Nov 1; 18(21):6058–64. [PubMed: 22988055]

30. DuBois SG, Marachelian A, Fox E, Kudgus RA, Reid JM, Groshen S, et al. Phase I Study of the Aurora A Kinase Inhibitor Alisertib in Combination With Irinotecan and Temozolomide for Patients With Relapsed or Refractory Neuroblastoma: A NANT (New Approaches to

Neuroblastoma Therapy) Trial. Journal of clinical oncology : official journal of the American Society of Clinical Oncology. 2016 Apr 20; 34(12):1368–75. [PubMed: 26884555]

31. Hubert CG, Rivera M, Spangler LC, Wu Q, Mack SC, Prager BC, et al. A Three-Dimensional Organoid Culture System Derived from Human Glioblastomas Recapitulates the Hypoxic Gradients and Cancer Stem Cell Heterogeneity of Tumors Found In Vivo. Cancer research. 2016 Apr 15; 76(8):2465–77. [PubMed: 26896279]
32. Shu Q, Wong KK, Su JM, Adesina AM, Yu LT, Tsang YT, et al. Direct orthotopic transplantation of fresh surgical specimen preserves CD133+ tumor cells in clinically relevant mouse models of medulloblastoma and glioma. Stem cells. 2008 Jun; 26(6):1414–24. [PubMed: 18403755]
33. Yu L, Baxter PA, Zhao X, Liu Z, Wadhwa L, Zhang Y, et al. A single intravenous injection of oncolytic picornavirus SVV-001 eliminates medulloblastomas in primary tumor-based orthotopic xenograft mouse models. Neuro-oncology. 2011 Jan; 13(1):14–27. [PubMed: 21075780]
34. Lindsay H, Huang Y, Du Y, Braun FK, Teo WY, Kogiso M, et al. Preservation of KIT genotype in a novel pair of patient-derived orthotopic xenograft mouse models of metastatic pediatric CNS germinoma. Journal of neuro-oncology. 2016 May; 128(1):47–56. [PubMed: 26956263]
35. Yu L, Baxter PA, Voicu H, Gurusiddappa S, Zhao Y, Adesina A, et al. A clinically relevant orthotopic xenograft model of ependymoma that maintains the genomic signature of the primary tumor and preserves cancer stem cells in vivo. Neuro-oncology. 2010 Jun; 12(6):580–94. [PubMed: 20511191]
36. Liu Z, Zhao X, Wang Y, Mao H, Huang Y, Kogiso M, et al. A patient tumor-derived orthotopic xenograft mouse model replicating the group 3 supratentorial primitive neuroectodermal tumor in children. Neuro-oncology. 2014 Jun; 16(6):787–99. [PubMed: 24470556]
37. Zhao X, Liu Z, Yu L, Zhang Y, Baxter P, Voicu H, et al. Global gene expression profiling confirms the molecular fidelity of primary tumor-based orthotopic xenograft mouse models of medulloblastoma. Neuro-oncology. 2012 May; 14(5):574–83. [PubMed: 22459127]
38. Zhao X, Zhao YJ, Lin Q, Yu L, Liu Z, Lindsay H, et al. Cytogenetic landscape of paired neurospheres and traditional monolayer cultures in pediatric malignant brain tumors. Neuro-oncology. 2015 Jul; 17(7):965–77. [PubMed: 25537021]
39. Liu Z, Zhao X, Mao H, Baxter PA, Huang Y, Yu L, et al. Intravenous injection of oncolytic picornavirus SVV-001 prolongs animal survival in a panel of primary tumor-based orthotopic xenograft mouse models of pediatric glioma. Neuro-oncology. 2013 Sep; 15(9):1173–85. [PubMed: 23658322]
40. Ulisse S, Delcros JG, Baldini E, Toller M, Curcio F, Giacomelli L, et al. Expression of Aurora kinases in human thyroid carcinoma cell lines and tissues. International journal of cancer. 2006 Jul 15; 119(2):275–82. [PubMed: 16477625]
41. Manfredi MG, Ecsedy JA, Chakravarty A, Silverman L, Zhang M, Hoar KM, et al. Characterization of Alisertib (MLN8237), an investigational small-molecule inhibitor of aurora A kinase using novel in vivo pharmacodynamic assays. Clinical cancer research : an official journal of the American Association for Cancer Research. 2011 Dec 15; 17(24):7614–24. [PubMed: 22016509]
42. Ahmad Z, Jasnos L, Gil V, Howell L, Hallsworth A, Petrie K, et al. Molecular and in vivo characterization of cancer-propagating cells derived from MYCN-dependent medulloblastoma. PloS one. 2015; 10(3):e0119834. [PubMed: 25785590]
43. Shu Q, Antalffy B, Su JM, Adesina A, Ou CN, Pietsch T, et al. Valproic Acid prolongs survival time of severe combined immunodeficient mice bearing intracerebellar orthotopic medulloblastoma xenografts. Clinical cancer research : an official journal of the American Association for Cancer Research. 2006 Aug 1; 12(15):4687–94. [PubMed: 16899619]
44. Detre S, Saclani Jotti G, Dowsett M. A "quickscore" method for immunohistochemical semiquantitation: validation for oestrogen receptor in breast carcinomas. Journal of clinical pathology. 1995 Sep; 48(9):876–8. [PubMed: 7490328]
45. Bao S, Wu Q, McLendon RE, Hao Y, Shi Q, Hjelmeland AB, et al. Glioma stem cells promote radioresistance by preferential activation of the DNA damage response. Nature. 2006 Dec 07; 444(7120):756–60. [PubMed: 17051156]

46. Pavon LF, Marti LC, Sibov TT, Malheiros SM, Brandt RA, Cavalheiro S, et al. In vitro Analysis of Neurospheres Derived from Glioblastoma Primary Culture: A Novel Methodology Paradigm. Frontiers in neurology. 2014 Jan 07.4:214. [PubMed: 24432012]
47. Wan F, Zhang S, Xie R, Gao B, Campos B, Herold-Mende C, et al. The utility and limitations of neurosphere assay, CD133 immunophenotyping and side population assay in glioma stem cell research. Brain pathology. 2010 Sep; 20(5):877–89. [PubMed: 20331619]
48. Laks DR, Masterman-Smith M, Visnyei K, Angenieux B, Orozco NM, Foran I, et al. Neurosphere formation is an independent predictor of clinical outcome in malignant glioma. Stem cells. 2009 Apr; 27(4):980–7. [PubMed: 19353526]
49. Chaichana K, Zamora-Berridi G, Camara-Quintana J, Quinones-Hinojosa A. Neurosphere assays: growth factors and hormone differences in tumor and nontumor studies. Stem cells. 2006 Dec; 24(12):2851–7. [PubMed: 16945995]
50. Venkatakrishnan K, Kim TM, Lin CC, Thye LS, Chng WJ, Ma B, et al. Phase 1 study of the investigational Aurora A kinase inhibitor alisertib (MLN8237) in East Asian cancer patients: pharmacokinetics and recommended phase 2 dose. Investigational new drugs. 2015 Aug; 33(4): 942–53. [PubMed: 26084989]
51. Kelly KR, Shea TC, Goy A, Berdeja JG, Reeder CB, McDonagh KT, et al. Phase I study of MLN8237—investigational Aurora A kinase inhibitor—in relapsed/refractory multiple myeloma, non-Hodgkin lymphoma and chronic lymphocytic leukemia. Investigational new drugs. 2014 Jun; 32(3):489–99. [PubMed: 24352795]
52. Van Brocklyn JR, Wojton J, Meisen WH, Kellough DA, Ecsedy JA, Kaur B, et al. Aurora-A inhibition offers a novel therapy effective against intracranial glioblastoma. Cancer research. 2014 Oct 01; 74(19):5364–70. [PubMed: 25106428]
53. Qi L, Zhang Y. Alisertib (MLN8237), a selective Aurora-A kinase inhibitor, induces apoptosis in human tongue squamous cell carcinoma cell both in vitro and in vivo. Tumour biology : the journal of the International Society for Oncodevelopmental Biology and Medicine. 2015 Mar; 36(3):1797–802. [PubMed: 25366143]
54. Asteriti IA, Di Cesare E, De Mattia F, Hilsenstein V, Neumann B, Cundari E, et al. The Aurora-A inhibitor MLN8237 affects multiple mitotic processes and induces dose-dependent mitotic abnormalities and aneuploidy. Oncotarget. 2014 Aug 15; 5(15):6229–42. [PubMed: 25153724]
55. Qi W, Spier C, Liu X, Agarwal A, Cooke LS, Persky DO, et al. Alisertib (MLN8237) an investigational agent suppresses Aurora A and B activity, inhibits proliferation, promotes endo-reduplication and induces apoptosis in T-NHL cell lines supporting its importance in PTCL treatment. Leukemia research. 2013 Apr; 37(4):434–9. [PubMed: 23153524]
56. Qi W, Cooke LS, Liu X, Rimsza L, Roe DJ, Manziolli A, et al. Aurora inhibitor MLN8237 in combination with docetaxel enhances apoptosis and anti-tumor activity in mantle cell lymphoma. Biochemical pharmacology. 2011 Apr 01; 81(7):881–90. [PubMed: 21291867]
57. Mahadevan D, Stejskal A, Cooke LS, Manziello A, Morales C, Persky DO, et al. Aurora A inhibitor (MLN8237) plus vincristine plus rituximab is synthetic lethal and a potential curative therapy in aggressive B-cell non-Hodgkin lymphoma. Clinical cancer research : an official journal of the American Association for Cancer Research. 2012 Apr 15; 18(8):2210–9. [PubMed: 22374334]
58. Kozyreva VK, Kiseleva AA, Ice RJ, Jones BC, Loskutov YV, Matalkah F, et al. Combination of Eribulin and Aurora A Inhibitor MLN8237 Prevents Metastatic Colonization and Induces Cytotoxic Autophagy in Breast Cancer. Molecular cancer therapeutics. 2016 Aug; 15(8):1809–22. [PubMed: 27235164]
59. Jensen JS, Omarsdottir S, Thorsteinsdottir JB, Ogmundsdottir HM, Olafsdottir ES. Synergistic cytotoxic effect of the microtubule inhibitor marchantin A from Marchantia polymorpha and the Aurora kinase inhibitor MLN8237 on breast cancer cells in vitro. Planta medica. 2012 Mar; 78(5): 448–54. [PubMed: 22331811]
60. Kelly KR, Ecsedy J, Medina E, Mahalingam D, Padmanabhan S, Nawrocki ST, et al. The novel Aurora A kinase inhibitor MLN8237 is active in resistant chronic myeloid leukaemia and significantly increases the efficacy of nilotinib. Journal of cellular and molecular medicine. 2011 Oct; 15(10):2057–70. [PubMed: 21091633]

61. Fiskus W, Hembruff SL, Rao R, Sharma P, Balusu R, Venkannagari S, et al. Co-treatment with vorinostat synergistically enhances activity of Aurora kinase inhibitor against human breast cancer cells. Breast cancer research and treatment. 2012 Sep; 135(2):433–44. [PubMed: 22825030]

Statement of translational relevance

Pediatric glioblastoma multiforme (pGBM) is a highly aggressive tumor with a poor prognosis despite multimodality therapy, thus new treatments are needed. We utilized a novel set of patient-derived orthotopic xenograft (PDOX) mouse models along with matching pairs of monolayer and neurospheres from different stage of clinical progression (diagnosis, recurrence, and terminal/autopsy). We detected Aurora A kinase (AURKA) over-expression in pGBM and identified MLN8237 (Alisertib) as an effective agent against a treatment naïve pGBM. Also our data involving 3 GBM models suggested that simultaneous inhibition of neurosphere and monolayer cells by MLN8237 correlated with prolonged animal survival. Additionally, decreased AURKA expression (due to intra-tumoral heterogeneity) and the presence of $CD133^{+}$ cells contributed to the recurrence or progression of pGBM xenografts following MLN8327 treatment. Since MLN8237 is a reversible inhibitor of AURKA that is administered orally and can cross the blood-brain barrier, our data support the use of MLN8237 in pGBMs and highlight the need for combination therapies.

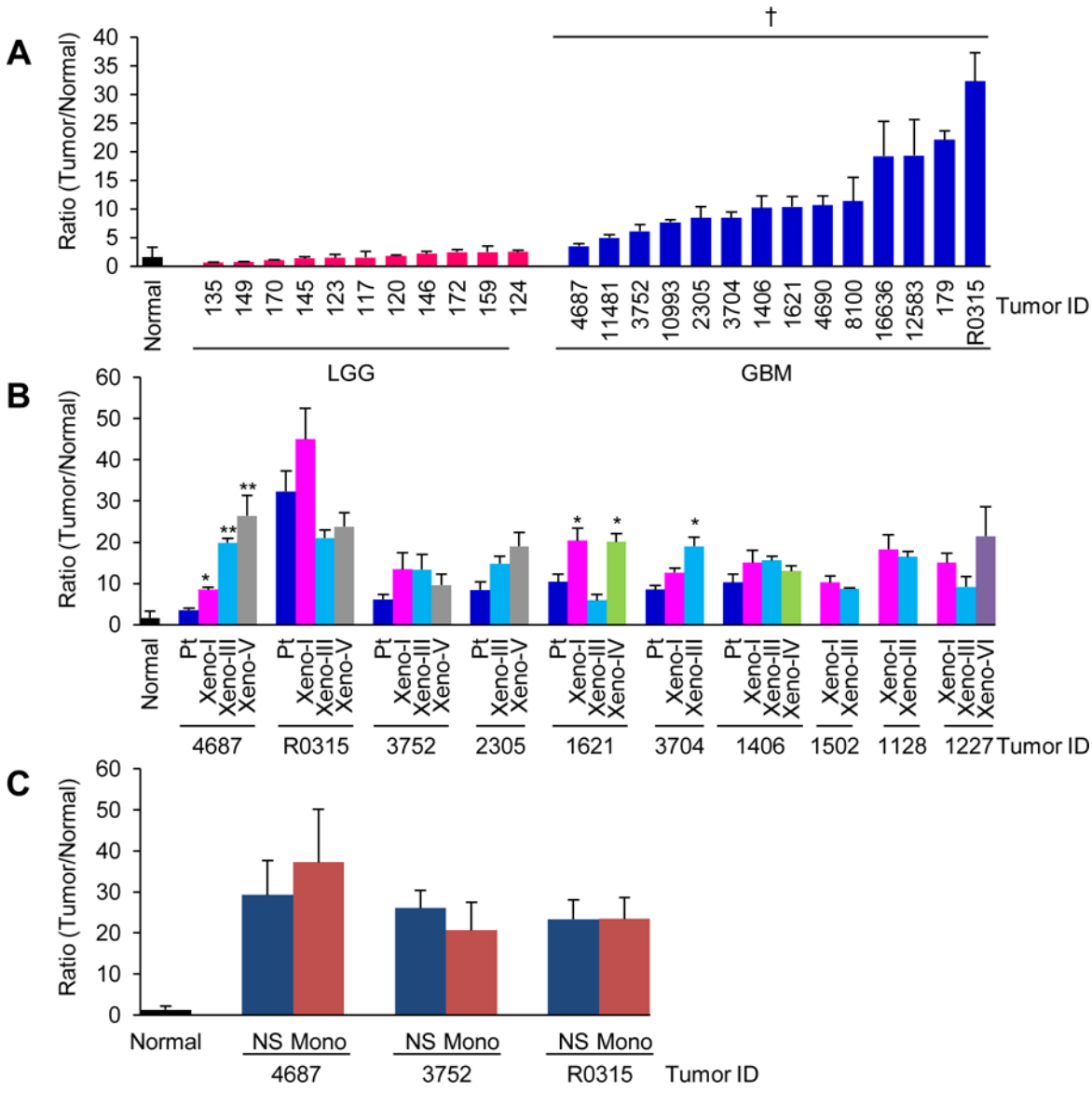

Figure 1. AURKA is overexpressed in tumors from patients with pGBM and in pGBM xenografts and cell lines

A. Levels of AURKA mRNA expression in pediatric LGG and pGBM patient tumor (***Pt***) samples normalized to normal cerebra. **B.** AURKA mRNA expression in patient and PDOX tumor samples of pGBM at various *in vivo* passages. **C.** AURKA mRNA expression in xenograft-derived paired monolayer (***Mono***) and neurosphere (***NS***) lines quantified by real-time PCR. Relative levels of AURKA were calculated with the AURKA/GAPDH ratio observed in normal cerebral tissues as 1. †P<0.001 in pGBM as compared to normal cerebral tissue and LGG. *P<0.05, **P<0.01 as compared to patient (***Pt***). There were no significant differences between neurospheres and monolayer cells in the 3 models.

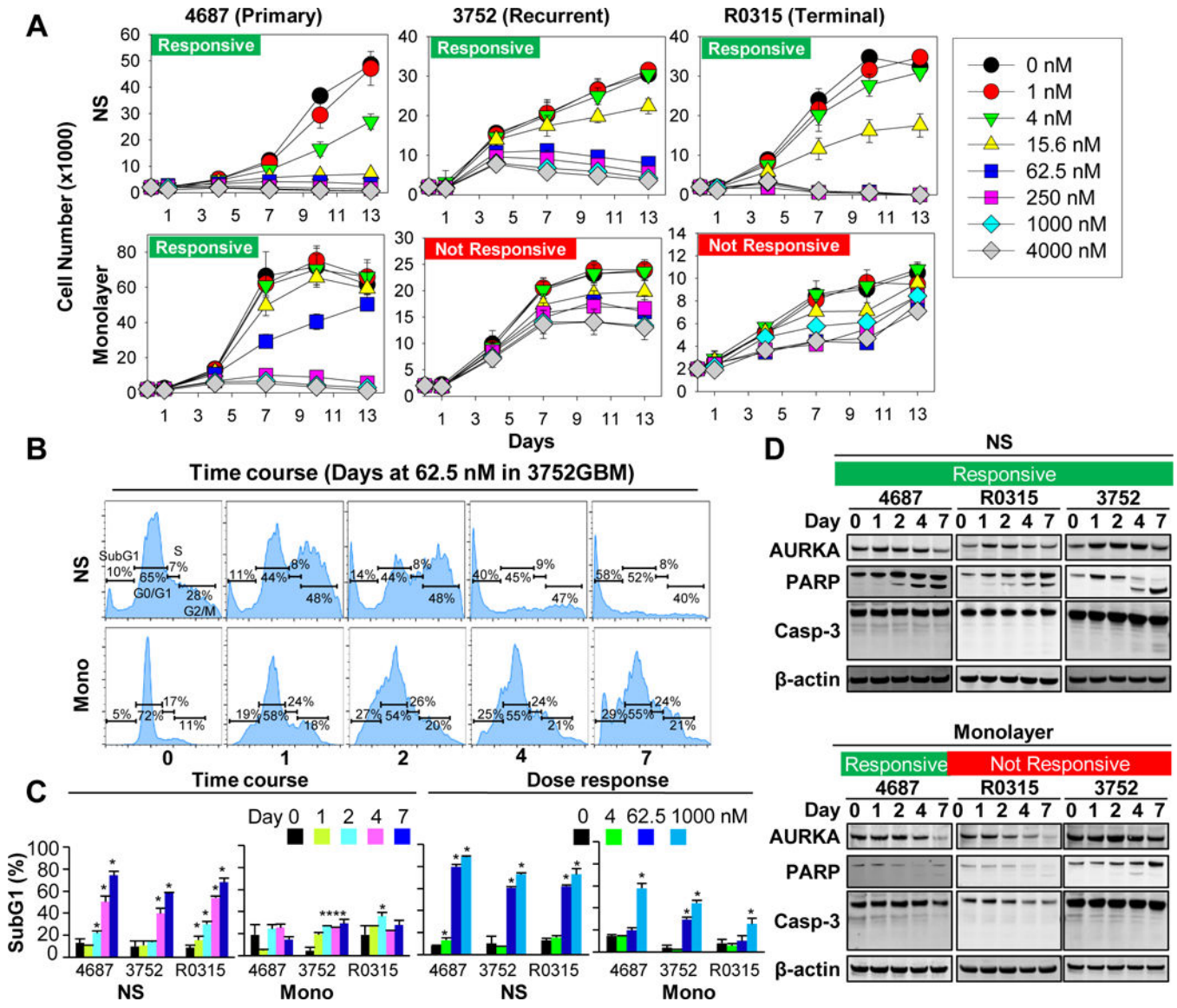

Figure 2. Anti-proliferative effects of MLN8237 through apoptosis in pGBM cell lines

A. Cells were exposed to varying concentrations of MLN8237 through day 13, and antitumor effects were examined by CCK8 assay in paired monolayer (***Mono***) and neurosphere (***NS***) in IC-4687GBM, IC-R0315GBM and IC-3752GBM. 2,000 cells/well. **B** and **C.** Paired monolayer (***Mono***) and neurosphere (***NS***) pGBM cell lines were treated with MLN8237 (62.5 nM) for time course and dose response at day 7 analyses. DNA was stained with Hoechst 33342 and analyzed with FCM. **B.** Representative DNA/RNA profiles in 3752GBM, time course at MLN8237 dose of 62.5 nM. **C.** Percentage of $SubG_1$ phase. †P<0.05. *P<0.01 compared to 0 nM. **D.** Western hybridization of AURKA, PARP, and caspase-3 with β-actin as loading control for time course treatment with 62.5 nM of MLN8237.

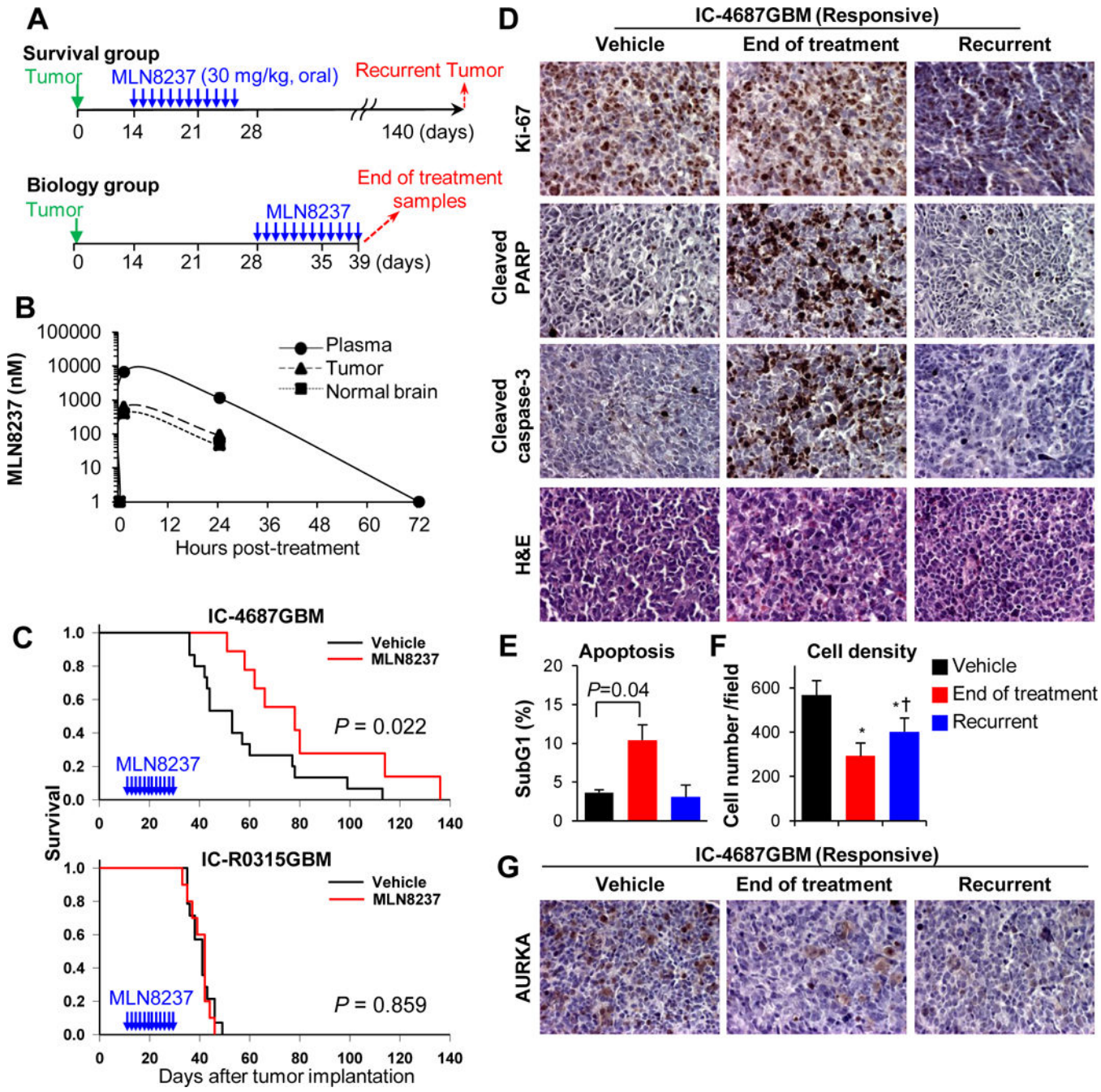

Figure 3. MLN8237 treatment significantly prolongs animal survival in a therapy-naïve IC-4687GBM model but not in a therapy-resistant model IC-R0315GBM

A. Treatment schema showing the grouping and timing of MLN8237 treatment. For the survival group, MLN8237 treatment (30 mg/kg/day, oral gavage x 12 days) was started two weeks post tumor implantation. When mice showed signs of neurological deficit (or become moribund), their brains were harvested and tumor tissues were collected (referred as the ***Recurrent Tumor***). For the biology group, the MLN8237 treatment (30 mg/kg/day, oral gavage x 12 days) was withheld for four weeks (to allow the xenograft tumors grew bigger to meet the need of biological assays), and the mouse brains harvested at the end of

treatment (referred as the ***End of Treatment*** *sample*). **B.** *In vivo* examination of MLN8237 concentration in mice bearing IC-4687GBM. Plasma, tumor, and normal brain were obtained from the biology group 1–72 hr post the last oral administration of MLN8237 and analyzed for MLN8237 concentration. **C.** Log-rank analysis of animal survival times. Mice (n=10-15/group) bearing IC-4687GBM or IC-R0315GBM were treated MLN8237 (***MLN8237***) and compared with those administered with vehicle (***Vehicle***). **D.** Representative immunohistochemical images of Ki-67, cleaved PARP, cleaved caspase-3, and H&E in IC-4687GBM. (Magnification: x40). **E.** MLN8237-induced apoptosis was detected as subG$_1$ in IC-4687GBM. DNA were stained with Hoechst 33342 followed by mouse antibody cocktail staining to gate out mouse cells. **F.** MLN8237 treatment decreases cell density in IC-4687GBM. Cell number/field was counted under x40 Magnification. *P<0.001 compared to vehicle. †P<0.001 compared to End of treatment. **G.** Representative immunohistochemical images of AURKA showing resistant tumor cells expressed low levels of AURKA in the recurrent tumor of IC-4687GBM. (Magnification: x40).

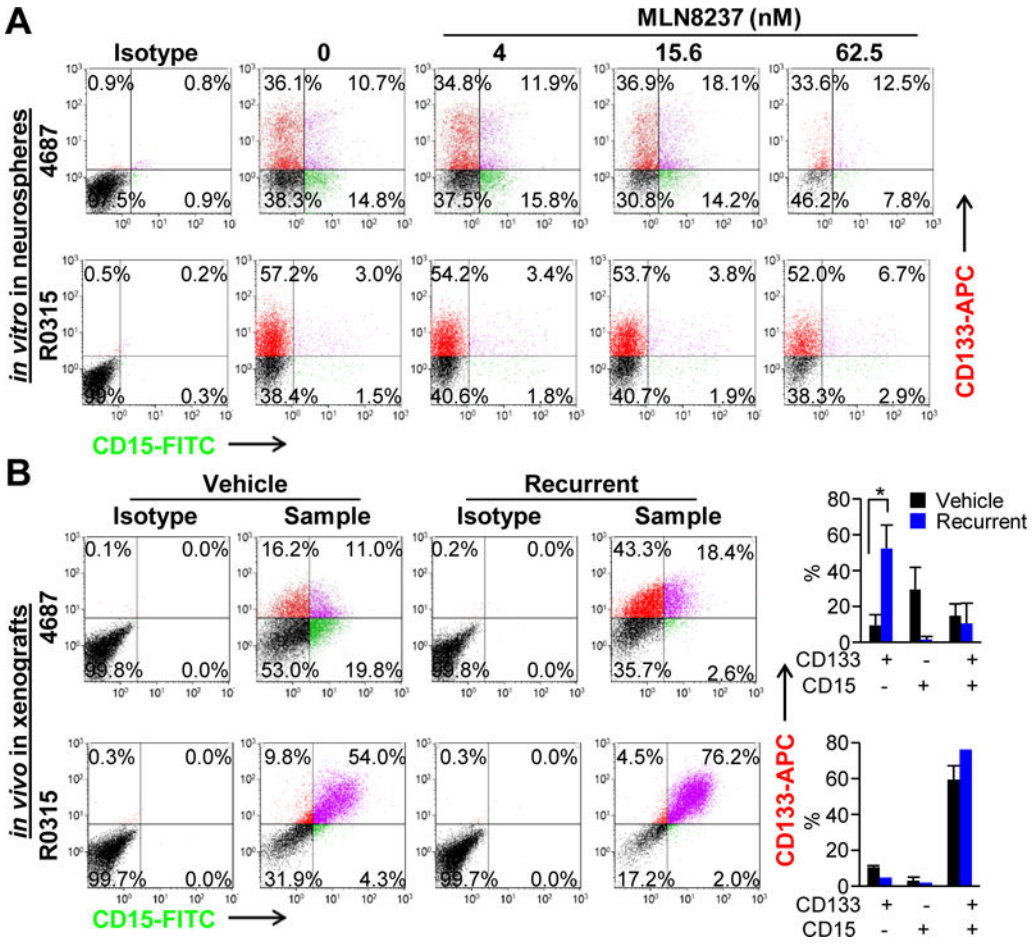

Figure 4. Effects of MLN8237 on the profile of putative CSCs *in vitro* and *in vivo*

A. *In vitro* dose response of $CD133^+$ and/or $CD15^+$ cells in IC-4687GBM (***4687***) and IC-R0315GBM (***R0315***) treated with MLN8237 (4-62.5 nM) for 7 days. **B.** Representative FCM profiles (*left panel*) and graphs of quantitative analysis (*right panel*) of *in vivo* changes of $CD133^+$ and/or $CD15^+$ cells. The vehicle treated xenografts (***Vehicle***) of IC-4687GBM (***4687***) and IC-R0315GBM (***R0315***) were compared with the recurrent tumors (***Recurrent***) that were harvested when the animals in the survival group were euthanized. Representative FCM profiles (*left panel*) and graphs of quantitative analysis (*right panel*) were presented. **P*=0.013.

Table 1

Patient clinical course

	4687GBM	3752GBM	R0315GBM
Clinical timepoint	**Initial**	**Recurrence**	**Autopsy**
Age	7 y	4 y	9 y
Gender	Male	Female	Female
Location	Right hemisphere and thalamus	Left frontal	Left parietal
Initial treatment	Subtotal resection **Sample obtained** Radiotherapy	Gross total resection Radiotherapy Temozolomide	Subotal resection Radiotherapy Temozolomide
Recurrence		Recurrent/progressive left frontal GBM at 5 months from diagnosis	Recurrent left parietal GBM at 8 months from diagnosis
1st relapse treatment	Peptide vaccine pilot study		Debulking and Cyberknife Procarbazine, Lomustine, and Vincristine Bevacizumab
Progression	Clinical tumor progression at 5 months from diagnosis	Further progression of tumor at 7 months from diagnosis	Further progression of tumor 14 months from diagnosis
Subsequent relapse treatment	Comfort care	Partial resection **Sample obtained** Phase I trial of vorinostat/ bortezomib	Comfort care
Autopsy			**Sample obtained**
P53 mutation	Not detected	Not detected	Not detected
H3K27 mutation	Not detected	Not detected	Not detected
Sample	**Previously untreated sample obtained from initial surgery**	**Sample obtained at repeat resection after primary and salvage treatment**	**Therapy-resistant autopsy sample**

Table 2

Summary of immunohistochemical characteristics of tumors from xenografts treated with MLN8237

		IC-4687GBM			IC-R0315GBM	
Molecule	**Target**	**Vehicle**	**At the end of treatment**	**Recurrent**	**Vehicle**	**Recurrent**
Ki-67	Cell proliferation	50%	60%	20-50%	35-50%	40-50%
Full PARP	Apoptosis	++ 4	+++ 4	+++ 4	+++ 4	+++ 4
Cleaved PARP	Apoptosis	+ 1	+++ 3	+ 1	+ 1	+++ 1
Full caspase-3	Apoptosis	+++ 4	+++ 4	+++ 4	+++ 4	+++ 4
Cleaved caspase-3	Apoptosis	++ 1	+++ 3	+ 1	++ 1	+++ 1

Scored intensity as negative (–), low (+), medium (++) and strongly positive (+++) and extent of immunopositivity as 0 = negative; 1 = 1–25%; 2 = 26 – 50%; 3 = 51 – 75%; 4 = >75% positive cells.